CONF-760810--2

LA-UR-76-917

TITLE: NUMERICAL CALCULATION OF TWO PHASE FLOW IN A SHOCK TUBE

AUTHOR(S): William C. Rivard
John R. Travis
Martin D. Torrey

SUBMITTED TO: Specialists Meeting on Transient
Two Phase Flow
Toronto, Ontario, CANADA
3 - 4 August 1976

los alamos
scientific laboratory
of the University of California
LOS ALAMOS, NEW MEXICO 87544

NUMERICAL CALCULATION OF TWO PHASE FLOW IN A SHOCK TUBE

by

W. C. Rivard
J. R. Travis
M. D. Torrey

University of California
Los Alamos Scientific Laboratory
Theoretical Division, Group T-3
Los Alamos, New Mexico 87545

Symbols

A	area of contact between phases per unit of mixture volume
$(E_g)_{cond}$	heat conduction term for the gas internal energy equation
$(E_\ell)_{cond}$	heat conduction term for the liquid internal energy equation
$(f_g)_{vis}$	viscous stress term for the gas momentum equation
$(f_\ell)_{vis}$	viscous stress term for the liquid momentum equation
H_g	specific enthalpy for the gas
I_g	specific internal energy for the gas
J_c	condensation rate
J_e	evaporation rate
K	interfacial friction function for momentum exchange
N	number of bubbles/droplets per unit of mixture volume
P	pressure
R	interfacial heat transfer function
R_u	universal gas constant
T_s	saturation temperature
T_g	gas temperature
T_ℓ	liquid temperature
$\underline{u}_g$	gas velocity
$\underline{u}_\ell$	liquid velocity
$(W_g)_{vis}$	viscous work term for the gas internal energy equation
$(W_\ell)_{vis}$	viscous work term for the liquid internal energy equation
θ	void fraction, volume of gas per unit of mixture volume
λ'_c	constant for the condensation rate J_c

λ_e	constant for the evaporation rate J_e
ρ_g	microscopic gas density, mass of gas per unit of gas volume
ρ'_g	macroscopic gas density, mass of gas per unit of mixture volume
ρ_ℓ	microscopic liquid density, mass of liquid per unit of liquid volume
ρ'_ℓ	macroscopic liquid density, mass of liquid per unit of mixture volume

ABSTRACT

Numerical calculations of the dynamics of initially saturated water-steam mixtures in a shock tube demonstrate the accuracy and efficiency of a new solution technique for the transient, two-dimensional, two-fluid equations. The dependence of the calculated results on time step and cell size are investigated. The effects of boiling and condensation on the flow physics suggest the merits of basic fluid dynamic measurements for the determination and evaluation of mass exchange models.

I. INTRODUCTION

The numerical calculation of transient two-phase flow has been receiving considerable attention recently because of its relevance to the safety analyses of nuclear power reactors. The dynamics of two phase flow is strongly governed by mass, momentum, and energy exchange between the phases. Consequently, numerical solution techniques that are highly implicit in these rate processes are required for accurate and efficient calculations. The results of calculations are presented in this paper for the two-phase flow of an initially saturated water-steam mixture in a shock tube. The purpose of this work is two fold. First, to demonstrate the accuracy and computational efficiency of a new solution technique[1] that solves the transient, two-fluid model equations in two space dimensions with a fully implicit treatment for all rate processes. The calculated results for a two phase mixture with equal velocities and temperatures and no phase change, hereafter referred to as a "frozen" two phase mixture, are compared to the known analytic solution[2] and excellent agreement is obtained. In particular, the propagation velocities for the rarefaction and shock waves through the two-phase mixture are accurately predicted. The effects of time step and cell size on the solutions obtained are studied for the frozen flow and for several different values of the boiling and condensation rates. The second purpose is to investigate the effects of phase change on the flow physics with a view toward establishing experiments that would assist the development of mass exchange models.

II. FIELD EQUATIONS AND SOLUTION METHODS

The liquid and gas dynamics are described by separate sets of field equations that are coupled through mass, momentum, and energy exchange and the assumption of pressure equilibrium between phases. The time-dependent, two-dimensional equations are

$$\frac{\partial \rho_g'}{\partial t} + \underline{\nabla} \cdot (\rho_g' \underline{u}_g) = J_e - J_c \quad , \tag{2.1}$$

$$\frac{\partial \rho_g' \underline{u}_g}{\partial t} + \underline{\nabla} \cdot (\rho_g' \underline{u}_g \underline{u}_g) = - \theta \underline{\nabla} p + K(\underline{u}_\ell - \underline{u}_g) + J_e \underline{u}_\ell - J_c \underline{u}_g + (\underline{f}_g)_{vis} \quad , \tag{2.2}$$

$$\frac{\partial \rho_g' I_g}{\partial t} + \underline{\nabla} \cdot (\rho_g' I_g \underline{u}_g) = - p\left[\frac{\partial \theta}{\partial t} + \underline{\nabla} \cdot (\theta \underline{u}_g)\right] + K(\underline{u}_g - \underline{u}_\ell)^2 + (J_e - J_c) H_g + R(T_\ell - T_g) + (W_g)_{vis} + (E_g)_{cond} \quad , \tag{2.3}$$

$$\frac{\partial \rho_\ell'}{\partial t} + \underline{\nabla} \cdot (\rho_\ell \underline{u}_\ell) = J_c - J_e \quad , \tag{2.4}$$

$$\frac{\partial \rho_\ell' \underline{u}_\ell}{\partial t} + \underline{\nabla} \cdot (\rho_\ell' \underline{u}_\ell \underline{u}_\ell) = - (1 - \theta) \underline{\nabla} p + K(\underline{u}_g - \underline{u}_\ell) + J_c \underline{u}_g - J_e \underline{u}_\ell + (\underline{f}_\ell)_{vis} \tag{2.5}$$

$$\frac{\partial \rho'_\ell I_\ell}{\partial t} + \underline{\nabla} \cdot (\rho'_\ell I_\ell \underline{u}_\ell) = - p \left\{ \frac{\partial}{\partial t} (1 - \theta) + \underline{\nabla} \cdot \left[(1 - \theta) \underline{u}_\ell \right] \right\}$$

$$- (J_e - J_c) H_g + R(T_g - T_\ell) + (W_\ell)_{vis}$$

$$+ (E_\ell)_{cond} \quad , \tag{2.6}$$

$$\rho'_g = \rho_g \theta \quad , \quad \rho'_\ell = (1 - \theta) \rho_\ell \quad , \tag{2.7}$$

$$\rho_g = \rho_g(p, I_g) \quad , \quad T_g = T_g(p, I_g) \quad , \tag{2.8}$$

$$\rho_\ell = \rho_\ell(p, I_\ell) \quad , \quad T_\ell = T_\ell(p, I_\ell) \quad . \tag{2.9}$$

These equations have been previously derived by Travis et al.[3] and are easily obtainable from the more detailed set suggested by Ishii.[4]

A numerical method for the solution of these equations in two-space dimensions was first proposed by Harlow and Amsden.[5] Their Implicit Multi-field (IMF) technique is valid for all flow speeds and for all degrees of coupling between the phases. A pressure iteration that uses the ICE technique to couple the gas continuity equation to the momentum equations with an additional implicit treatment of the momentum exchange term is the basis of the technique. The liquid continuity equation and the two internal energy equations are solved explicitly prior to the pressure iteration. The effects of phase change are included after the pressure iteration.

Experience with the KACHINA code,[6] which utilizes this solution technique, has shown the need to include mass exchange and the liquid continuity equation within the implicit pressure iteration to alleviate severe restrictions in the computational time step for certain cases. A new computer code, K-FIX, has been written for this purpose. K-FIX implicitly solves both

continuity equations, both momentum equations, and the portions of both internal energy equations that account for changes in internal energy due to rate processes. Momentum convection and viscous stresses may be easily included within the pressure iteration or evaluated explicitly before it. The effects of energy convection, work, and heat conduction on the internal energies are included after the pressure iteration. Details of the K-FIX solution methodology and the code description are contained in ref. 1. Calculations with K-FIX on a variety of problems has shown that accurate results are obtained with time steps that can often be an order of magnitude larger than were possible with KACHINA. The inclusion of both continuity equations within the pressure iteration provides a continuous dependence of the solution upon the void fraction particularly near the limits of no void and total void.

III. RESULTS

The results of calculations with K-FIX are presented here for a shock tube that is initially filled with saturated water-steam mixtures at pressures of 0.5 MPa and 0.1 MPa separated by a diaphragm. The mixtures are considered homogeneous with a void fraction of 0.05 in the high pressure region and 0.10 in the low pressure region. The interfacial friction coefficient K and the interfacial heat transfer coefficient R were set large in all cases so that the velocities and temperatures of the two phases would be very nearly equal. The state equations that describe the thermodynamic properties of water and steam are given in ref. 7. The phase change rates for boiling and condensation are also given in ref. 7 and are repeated here for convenience

$$J_e = \lambda_e A \rho'_\ell \theta (T_s R_u)^{\frac{1}{2}} (T_\ell - T_s)/T_s \ , \quad \text{for} \quad T_\ell \geq T_s$$
$$= 0 \ , \text{otherwise} \qquad (3.1)$$

$$J_c = \lambda_c A \rho'_g (1-\theta) (T_s R_u)^{\frac{1}{2}} (T_s - T_g)/T_s \ , \quad \text{for} \quad T_g \leq T_s$$
$$= 0 \ , \text{otherwise} \qquad (3.2)$$

where A is proportional to the area of contact between the two phases per unit of mixture volume. For N equal size spherical bubbles or droplets per unit volume, A is given by

$$A = \begin{cases} \theta^{2/3} (4\pi N)^{1/3} \ , & \theta \leq 1/2 \\ (1-\theta)^{2/3} (4\pi N)^{1/3} \ , & \theta > 1/2 \ . \end{cases} \qquad (3.3)$$

These expressions are known to neglect certain essential elements of the microphysics of phase change, e.g., the effects of heat conduction, but they do contain sufficient physics for our present purposes.

Calculations were performed first for the frozen two-phase mixture by setting the phase change rates identically equal to zero. The results of these calculations, with a time step of $\delta t = 100 \mu s$ and a cell size of $\delta z = 10$ mm are compared to the analytic solution of Wendroff (see ref. 2). Figures 3.1a - c show profiles of pressure, void fraction, and velocity at a time of 2 ms after the diaphragm, which is initially positioned at $z = 0.5$ m, is ruptured. The results of the numerical calculation (solid line) are in excellent agreement with the analytic solution (dashed line). The shock propagates to the right with a velocity of 54.8 m/s into a mixture with a sound speed of 33.9 m/s.* In the compressed state behind the

*The sound speed corresponds to the propagation velocity of small disturbances through the mixture under the conditions of velocity and temperature equilibrium between phases according to ref. 2.

shock the void fraction is 0.0408, the pressure is 0.261 MPa, and the liquid and gas velocities are 3.38 m/s. The rarefaction propagates to the left with a speed of 104.0 m/s at its head and a speed of 53.7 m/s at its tail. The speed of the rarefaction head corresponds to the sound speed in the frozen two-phase mixture, which is considerably less than the sound speed in either pure water, 1.23 Km/s, or pure steam, 0.582 Km/s.

The dependence of the calculated results upon the cell size and time step was investigated by performing additional calculations. The effects of time step were studied by holding the cell size fixed at $\delta x = 10$ mm and reducing the time step to $\delta t = 10\mu s$ and then to $\delta t = 1\mu s$. The pressure profiles obtained are shown in Figs. 3.2a - b for comparison. The results are generally unchanged but slightly more accurate, particularly in the rarefaction, due to the improved integration in time. With the smaller time steps, sound signals propagate much less than one cell per cycle and hence are more accurately followed as they move through the computing mesh. With these small time steps the implicit solution technique reduces essentially to an explicit scheme. The state beind the shock and the shock position are essentially unchanged. The effects of cell size were studied by holding the time step constant at $\delta t = 100\mu s$ and reducing the cell size to $\delta z = 5$ mm and then to $\delta z = 2.5$ mm. The pressure profiles that were obtained are shown in Figs. 3.3a - b and are essentially identical with that obtained for $\delta z = 10$ mm.

The effects of phase change upon the fluid dynamics were investigated by considering separately the effects due to boiling and then the effects due to condensation. Calculations with both boiling and condensation

occurring simultaneously were also made and their results are presented later. To investigate the effects of boiling alone, calculations were performed for various values of λ_e with the condensation rate set identically to zero. Figures 3.4a - d show the profiles of pressure, void fraction, velocity, and mass exchange rate $(J_e - J_c)$ at a time of 2 ms for $\lambda_e = 0.01$. The profiles are much different than those obtained without phase change. Boiling has raised the pressure at the tail of the rarefaction so that the shock is significantly stronger. The shock pressure and the shock velocity are increased 72% and 32% respectively over their values without phase change. The rarefaction, on the other hand, is significantly weakened and its penetration to the left is reduced as the system boils towards equilibrium, which raises the pressure and reduces the difference between the liquid and saturation temperatures. The void fraction increases rapidly in the region where boiling is occurring due to the production of vapor and the displacement of liquid to the right, which destroys the concept of a "contact surface." The velocity profile is much narrower than in the case without phase change and is no longer nearly symmetric about the position $z = 0.5$ m. The effect of changing the boiling rate is seen in Figs. 3.5a - b. The pressure profile in Fig. 3.5a corresponds to a boiling rate with $\lambda_e = 0.001$ while the pressure profile in Fig. 3.5b was obtained for $\lambda_e = 0.1$. At the lower boiling rate the pressure profile is intermediate between that obtained with $\lambda_e = 0.01$ and that obtained without phase change. The shock is strengthening while the rarefaction is weakening. The void fraction peaks at $\theta = 0.19$ and the maximum velocity is 4.72 m/s. The boiling rate with $\lambda_e = 0.1$ is an infinite rate for practical purposes. The liquid and saturation temperatures are equal to within 0.15°K compared to differences as large as 10°K for $\lambda_e = 0.001$.

The strength of the shock no longer increases as λ_e is increased above a value of 0.1. The void fraction peaks at about $\theta = 0.52$ and the maximum velocity is 5.86 m/s.

These calculations with boiling only were made with a cell size of 5 mm and a time step of 100μs. The results are essentially unchanged as the time step and cell size are individually reduced. A cell size of 5 mm was used for these results instead of the previous value of 10 mm because of a change in detail of the pressure step at $z = 0.5$ m with the larger cell size. In practice this change is small enough to be of no real concern, but is simply the normal loss of detail that occurs with decreased spatial resolution.

The effects of condensation alone were studied for various values of the coefficient λ_c with the boiling rate set identically to zero. Figures 3.6a - d show the calculated profiles of pressure, void fraction, velocity, and mass exchange rate at a time of 2.0 ms for $\lambda_c = 100$. The results show a decrease in shock pressure that is accompanied by a decrease in shock velocity. The pressure behind the shock is reduced by 10% and the shock velocity is reduced by 28% when compared to their values without phase change. The void fraction is reduced to nearly zero behind the shock by the condensation of steam and the influx of liquid from the left. Expansion through the rarefaction is increased to match the lower shock pressure, which leads to higher fluid velocity. The small velocity step at about $z = 0.5$ m results from the sharp rise in void fraction and the condition, from the liquid continuity equation, that $\underline{\nabla} \cdot (1 - \theta)\, \underline{u}_\ell$ should very nearly vanish. Condensation occurs very rapidly across the shock for this value of λ_c and is limited in magnitude behind the shock by the very small void.

Pressure profiles for $\lambda_c = 10$ and $\lambda_c = 1$ are shown for comparison in Figs. 3.7a - b respectively. For $\lambda_c = 1$, the shock velocity is reduced by 21% compared with its value without phase change. Also, no constant state exists in the region between the shock and rarefaction tail, since significant condensation is occurring throughout this region. The void fraction decreases gradually to a minimum value of 0.013 between the shock front and about the position $z = 0.5$ m. The profiles for $\lambda_c = 10$ are intermediate to those with $\lambda_c = 1$ and those with $\lambda_c = 100$.

The results shown were obtained with a time step of 100μs and a cell size of 2.5 mm and are essentially invariant as δt and δz are reduced. For a cell size of 10 mm, however, large variations occur in the solution as the time step is reduced. Similarly, for a time step of 100μs large variations occur as the cell size is increased to 10 mm. Figures 3.8a - b show profiles of pressure obtained with $\delta t = 100\mu s$, $\delta z = 10$ mm and $\delta t = 10\mu s$, $\delta z = 10$ mm respectively, to illustrate these solution variations. The shock pressure varies periodically in time with a period equal to the transit time of the shock from one cell center to the next. In Fig. 3.8b the full pressure rise for the shock occurs across a single cell, which is indicative of insufficient spatial resolution. Condensation causes these solution variations when the rate is sufficiently high that the void fraction is reduced to near zero in a time that is short compared to the transit time of material through the shock. The minimum transit time occurs when the shock is one cell thick and is given by $\delta z/U$ where U is the shock speed. When the void fraction is reduced to nearly zero the liquid continuity equation requires that $\underline{V} \cdot \underline{u}_\ell$ be very nearly zero. Since the shock is by nature compressive, this cannot occur within the shock. Consequently, in an attempt to alleviate

this situation, the shock pressure rises to accelerate the shock and reduce its thickness.

The results of calculations for both boiling and condensation with $\lambda_e = 0.01$ and $\lambda_c = 100$ are shown in Figs. 3.9a - d. The pressure profile is dominated by the effects of boiling. The shock strength is substantially increased and the rarefaction is substantially weakened. The void fraction profile clearly reflects the combined effects. A near zero void resides behind the shock where condensation is occurring while a large void exists near the rarefaction tail due to boiling. The combined effects of boiling and condensation result in a much steeper and somewhat stronger spike in void fraction than occurred with boiling alone. The spike in the velocity profile results directly from this and the previously mentioned condition from the liquid continuity equation that $\nabla \cdot ((1 - \theta)\, \underline{u}_\ell) \approx 0$. The peak condensation rate through the shock is larger than for condensation alone due to the increase in shock pressure compared with the result in Fig. 3.6a. Similarly, the peak boiling rate is larger than for boiling alone due to the decrease in pressure near the rarefaction tail compared with the result in Fig. 3.4a. The small spike in pressure at about $z = 0.5$ m is due to the high condensation rate there that results from the influx of steam from the left. The results shown were obtained with $\delta t = 100\,\mu s$ and $\delta z = 2.5$ mm. Further reductions in time step and cell size produce no significant changes in the results.

IV. SUMMARY

Numerical calculations with the K-FIX code have been made for the transient, two-phase fluid dynamics in a shock tube using a two-fluid model. The results are compared with an analytic solution, which is valid in the absence of phase change, and excellent agreement is obtained. The effects of boiling and condensation upon the fluid dynamics are shown for different phase change rates. As the shock passes through the initially saturated mixture, condensation takes place through the shock and behind it, which reduces the shock pressure and velocity. On the other hand, as the rarefaction propagates into the saturated mixture boiling occurs, which tends to restore the pressure and hence reduce the propagation velocity of the rarefaction head. The results demonstrate the efficiency and accuracy of the highly implicit solution method used in K-FIX. The importance of spatial resolution through the shock is demonstrated when the shocked material undergoes condensation. As the condensation rate is increased, the cell size must be reduced so that the transit time for material through the shock is on the order of the e-folding time for void reduction. The calculational results are invariant to reductions in time step and cell size once adequate spatial resolution is achieved. The sensitivity of the fluid dynamics to changes in the boiling and condensation rates strongly suggests that basic fluid dynamic measurements would provide valuable data for establishing mass exchange rates.

REFERENCES

1. Rivard, W. C. and Torrey, M. D., "K-FIX: A Computer Program for Transient, Two-Dimensional, Two-Fluid, Flow with Mass Exchange," Los Alamos Scientific Laboratory report (in preparation).

2. Wendroff, B., "Shock Propagation in Variable Area Ducts with Phase Changes: An Extension of Chisnell's Method," J. Eng. Math. (submitted for publication) (LA-UR-76-851).

3. Travis, J. R., Harlow, F. H., and Amsden, A. A., "Numerical Calculation of Two-Phase Flows," Los Alamos Scientific Laboratory report LA-5942-MS (1975); also accepted for publication in Nuclear Science and Engineering.

4. Ishii, M., Thermo-Fluid Dynamic Theory of Two-Phase Flow, Eyrolles 183 (1975).

5. Harlow, F. H. and Amsden, A. A., "Numerical Calculation of Multiphase Fluid Flow," J. Comp. Phys. 17, 19 (1975).

6. Amsden, A. A. and Harlow, F. H., "KACHINA: An Eulerian Computer Program for Multifield Fluid Flows," Los Alamos Scientific Laboratory report LA-5680 (1974).

7. Rivard, W. C. and Torrey, M. D., "Numerical Calculation of Flashing from Long Pipes Using a Two-Field Model," Los Alamos Scientific Laboratory report LA-6104-MS (1975).

Figure Captions:

Fig. 3.1a. Pressure profiles at t = 2 ms without phase change.

Fig. 3.1b. Volume fraction of void profiles at t = 2 ms without phase change.

Fig. 3.1c. Velocity of liquid and gas profiles at t = 2 ms without phase change.

Fig. 3.2a. Pressure at t = 2 ms for $\delta t = 10\mu s$, $\delta z = 10$ mm without phase change.

Fig. 3.2b. Pressure at t = 2 ms for $\delta t = 1\mu s$, $\delta z = 10$ mm without phase change.

Fig. 3.3a. Pressure at t = 2 ms for $\delta t = 100\mu s$, $\delta z = 5$ mm without phase change.

Fig. 3.3b. Pressure at t = 2 ms for $\delta t = 100\mu s$, $\delta z = 2.5$ mm without phase change.

Fig. 3.4a. Pressure at t = 2 ms with boiling only.

Fig. 3.4b. Volume fraction of void at t = 2 ms with boiling only.

Fig. 3.4c. Velocity of liquid and gas at t = 2 ms with boiling only.

Fig. 3.4d. Mass exchange rate at t = 2 ms with boiling only.

Fig. 3.5a. Pressure at t = 2 ms for $\lambda_e = 0.001$ with boiling only.

Fig. 3.5b. Pressure at t = 2 ms for $\lambda_e = 0.1$ with boiling only.

Fig. 3.6a. Pressure at t = 2 ms with condensation only.

Fig. 3.6b. Volume fraction of void at t = 2 ms with condensation only.

Fig. 3.6c. Velocity of liquid and gas at t = 2 ms with condensation only.

Fig. 3.6d. Mass exchange rate at t = 2 ms with condensation only.

Fig. 3.7a. Pressure at t = 2 ms for $\lambda_c = 10$ with condensation only.

Fig. 3.7b. Pressure at t = 2 ms for $\lambda_c = 1$ with condensation only.

Fig. 3.8a. Pressure at t = 2 ms for $\delta t = 100\mu s$, $\delta z = 10$ mm with condensation only.

Fig. 3.8b. Pressure at $t = 2$ ms for $\delta t = 10\mu s$, $\delta z = 10$ mm with condensation only.

Fig. 3.9a. Pressure at $t = 2$ ms with boiling and condensation.

Fig. 3.9b. Volume fraction of void at $t = 2$ ms with boiling and condenation.

Fig. 3.9c. Velocity of liquid and gas at $t = 2$ ms with boiling and condensation.

Fig. 3.9d. Mass exchange rate at $t = 2$ ms with boiling and condensation.

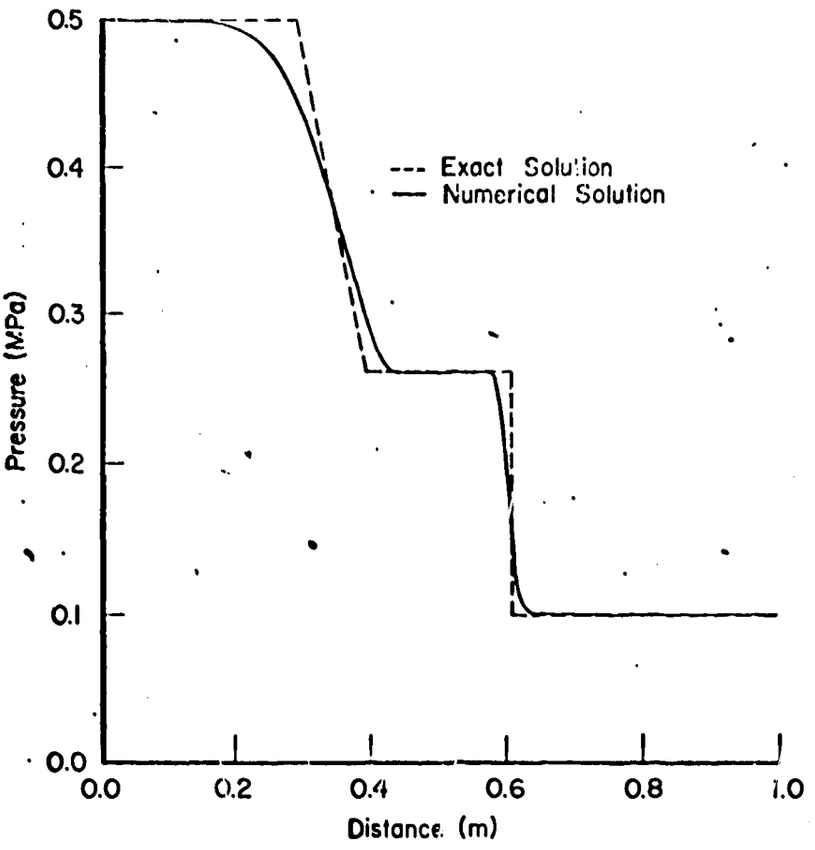

Fig. 3.1a. Pressure profiles at t = 2 ms without phase change.

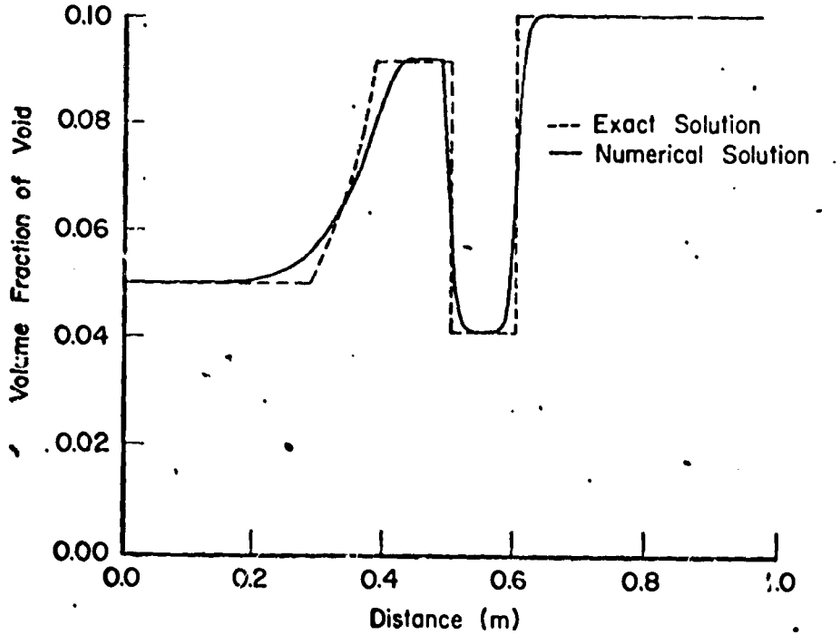

Fig. 3.1b. Volume fraction of void profiles at t = 2 ms without phase change.

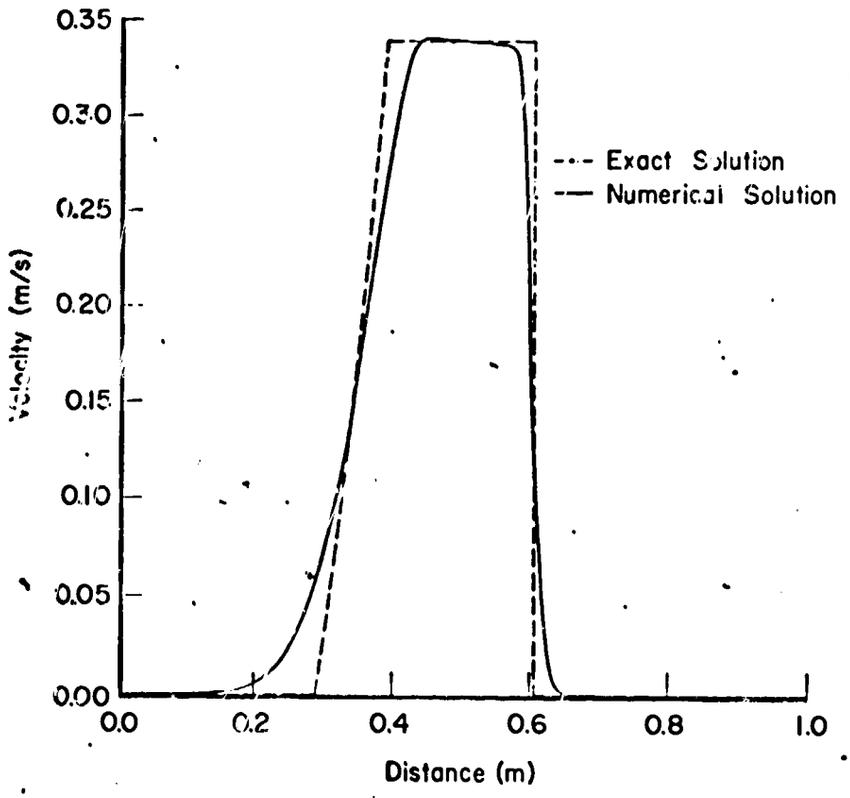

Fig. 3.1c. Velocity of liquid and gas profiles at t = 2 ms without phase change.

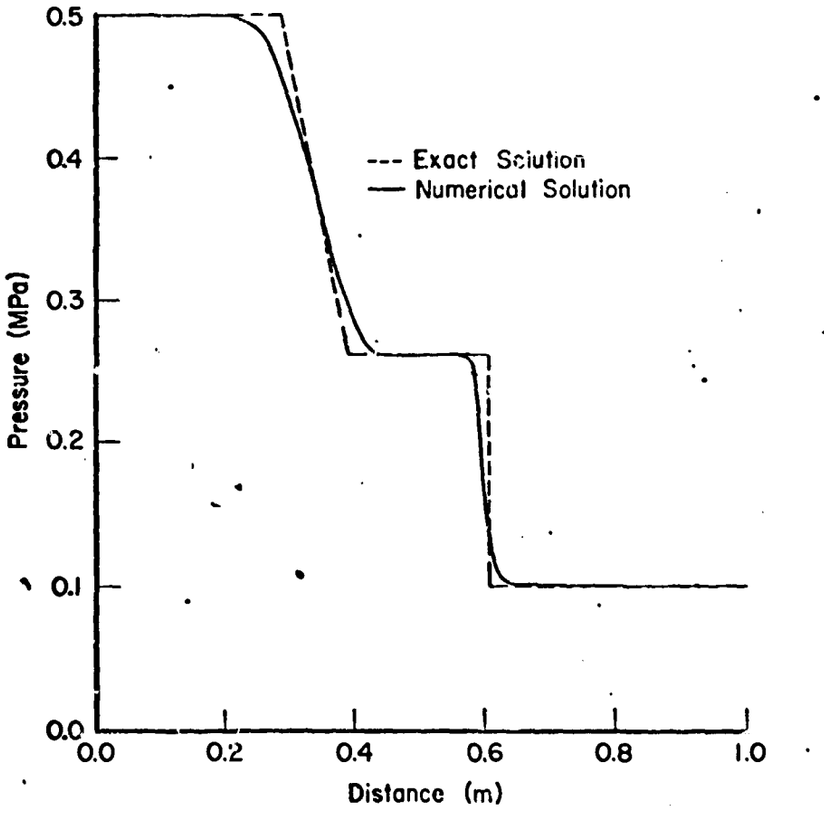

Fig. 3.2a. Pressure at $t = 2$ ms for $\delta t = 10\mu s$, $\delta z = 10$ mm without phase change.

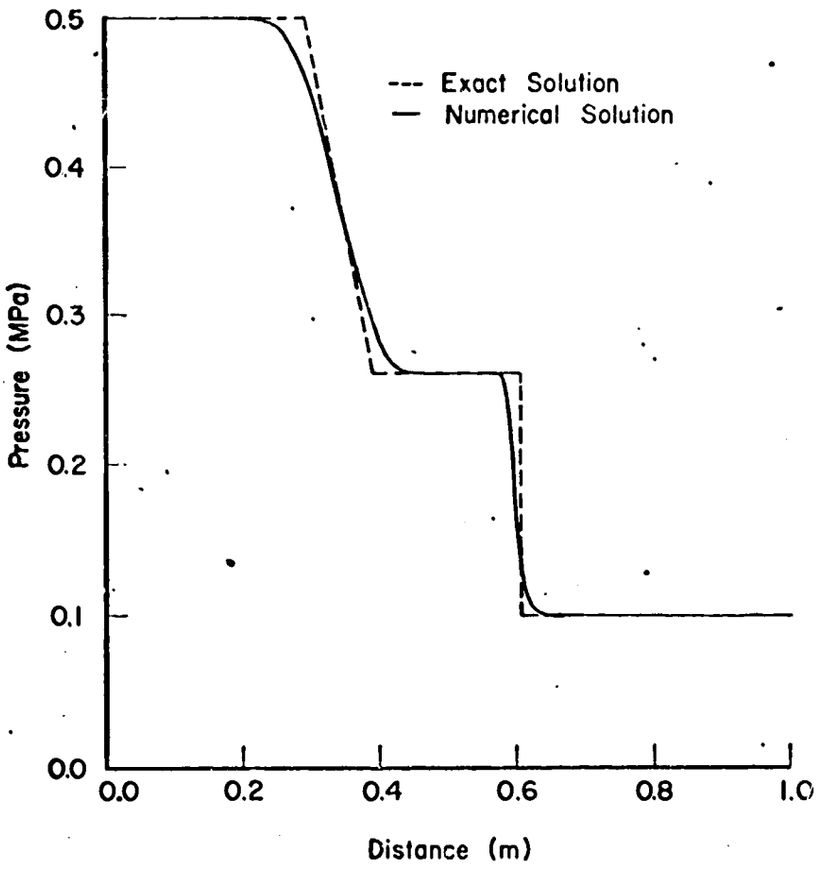

Fig. 3.2b. Pressure at $t = 2$ ms for $\delta t = 1\mu s$, $\delta z = 10$ mm without phase change.

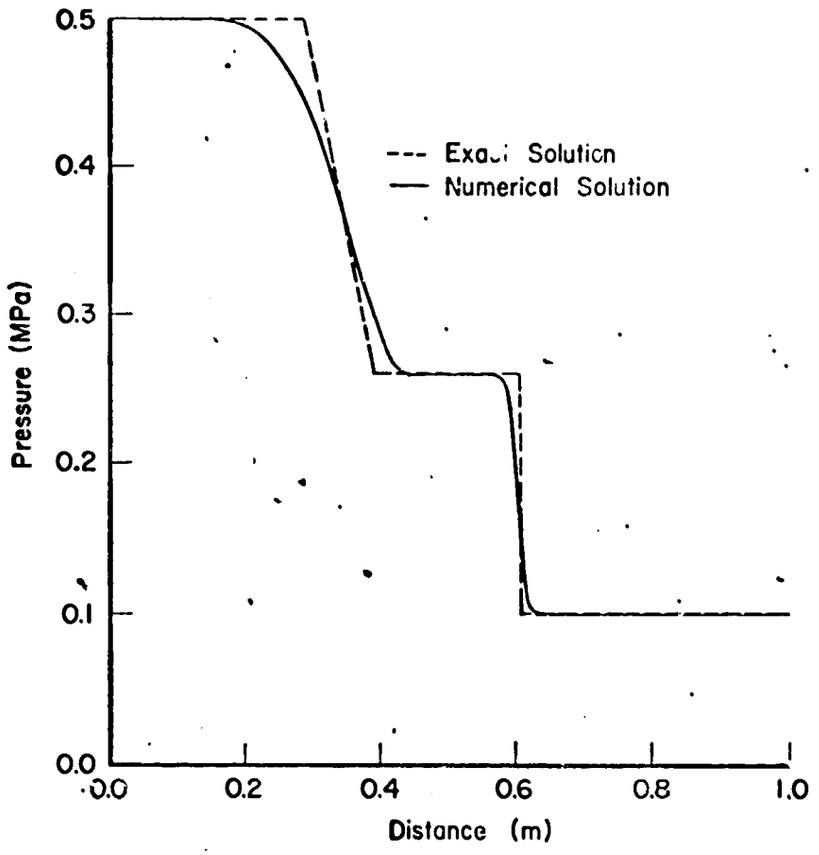

Fig. 3.3a. Pressure at $t = 2$ ms for $\delta t = 100\mu s$, $\delta z = 5$ mm without phase change.

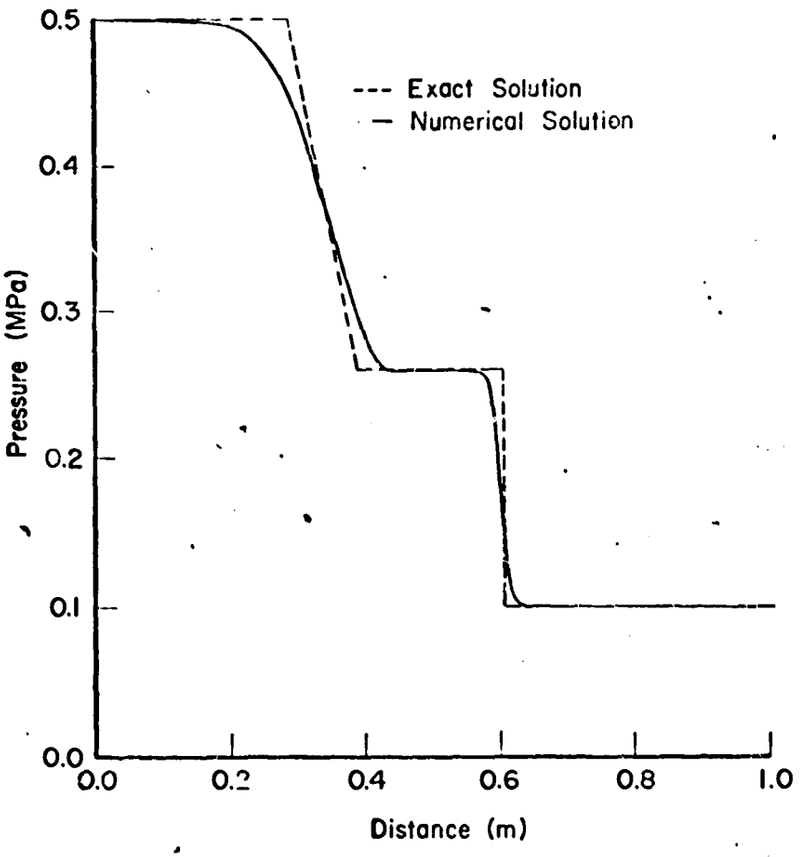

Fig. 3.3b. Pressure at t = 2 ms for $\delta t = 100\mu s$, $\delta x = 2.5$ mm without phase change.

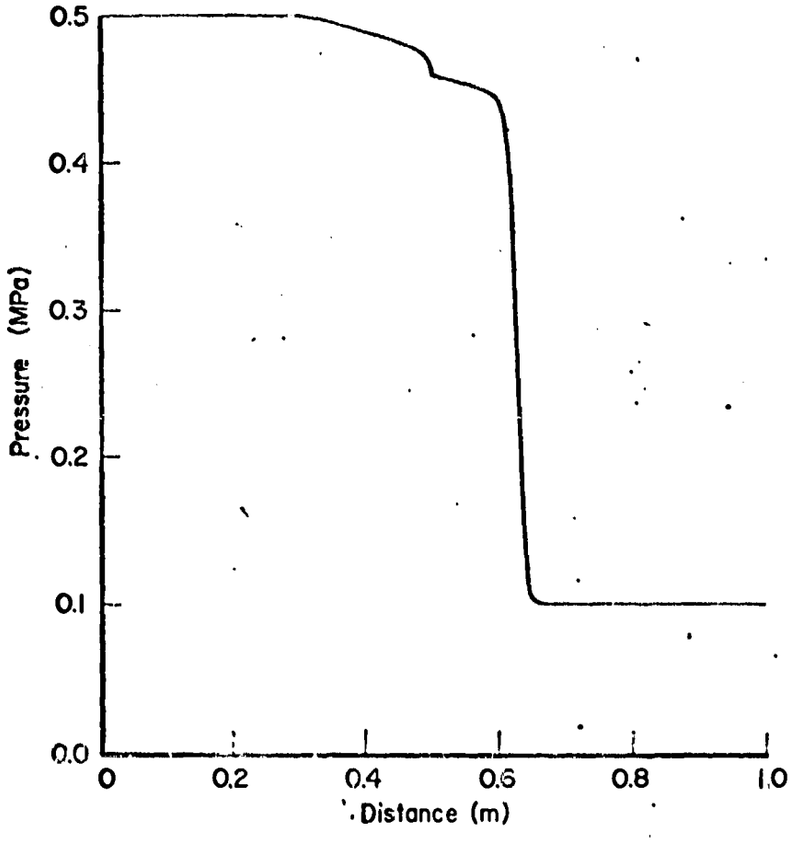

Fig. 3.4a. Pressure at t = 2 ms with boiling only.

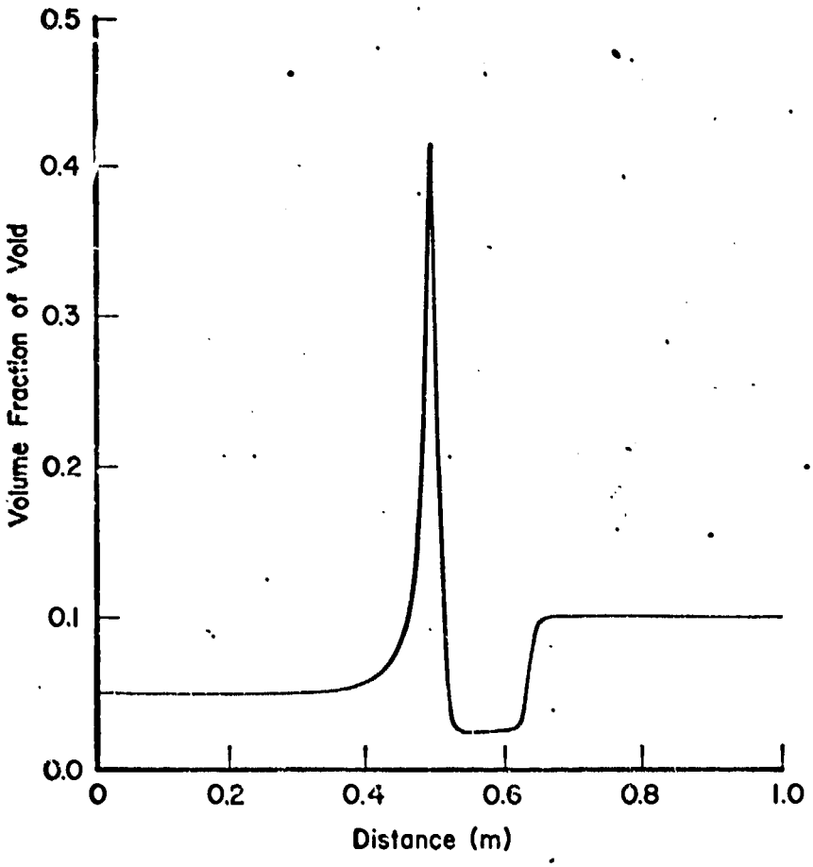

Fig. 3.4b. Volume fraction of void at t = 2 ms with boiling only.

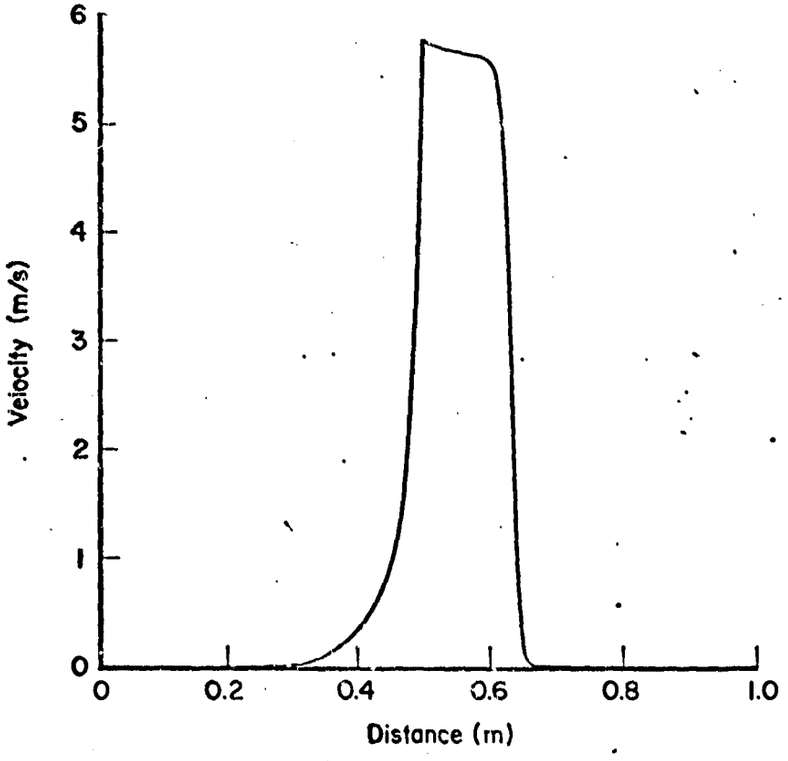

Fig. 3.4c. Velocity of liquid and gas at t = 2 ms with boiling only.

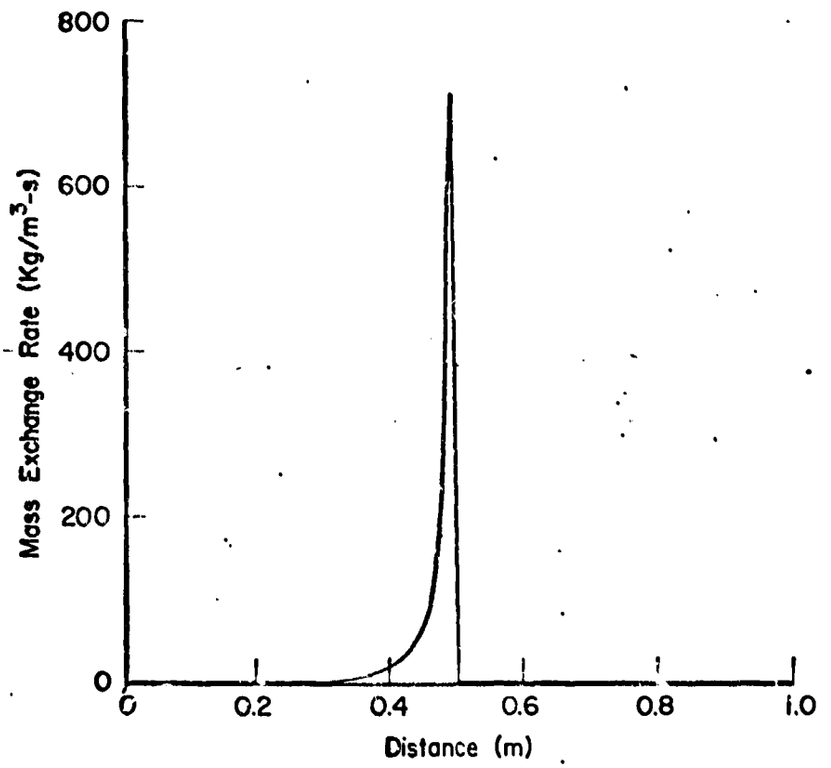

Fig. 3.4d. Mass exchange rate at t = 2 ms with boiling only.

3.5a

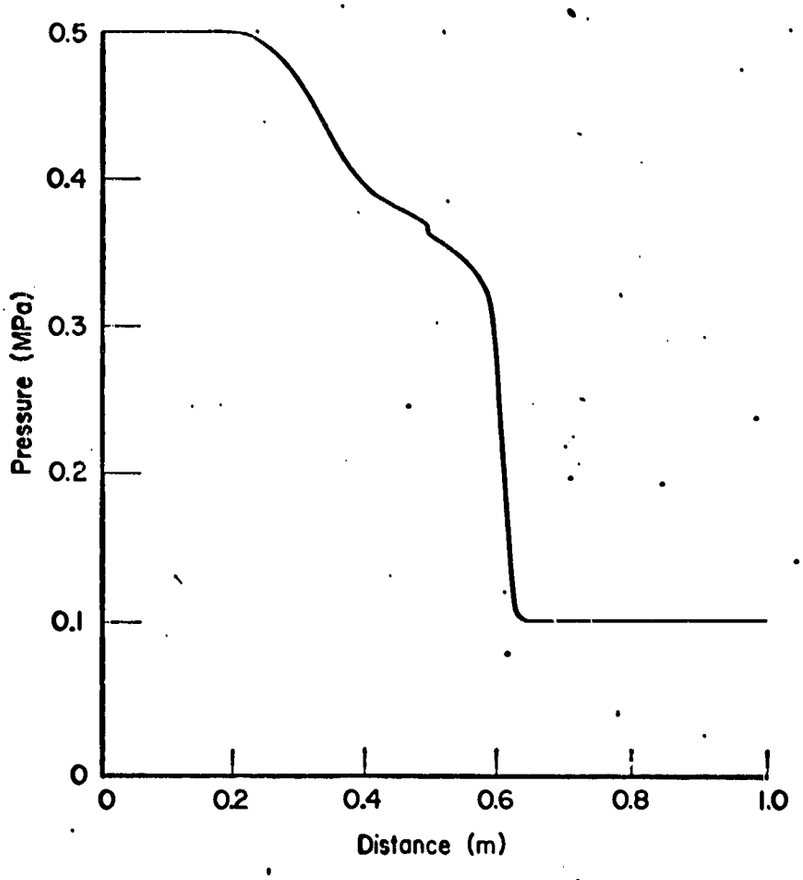

Fig. 3.5a. Pressure at t = 2 ms for $\lambda_e = 0.001$ with boiling only.

3.5b

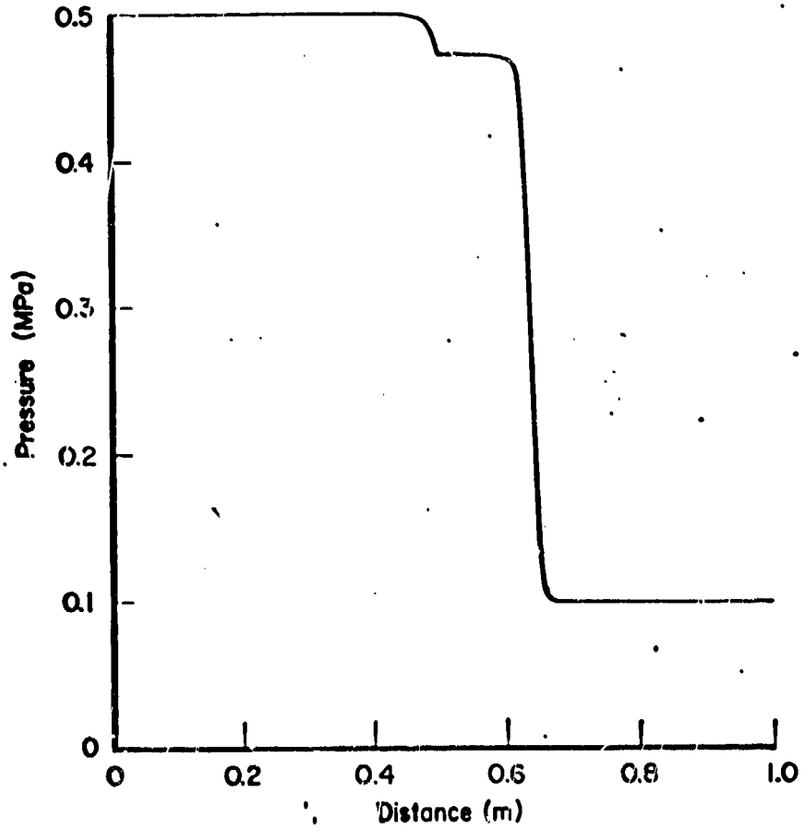

Fig. 3.5b. Pressure at t = 2 ms for λ = 0.1 with boiling only.

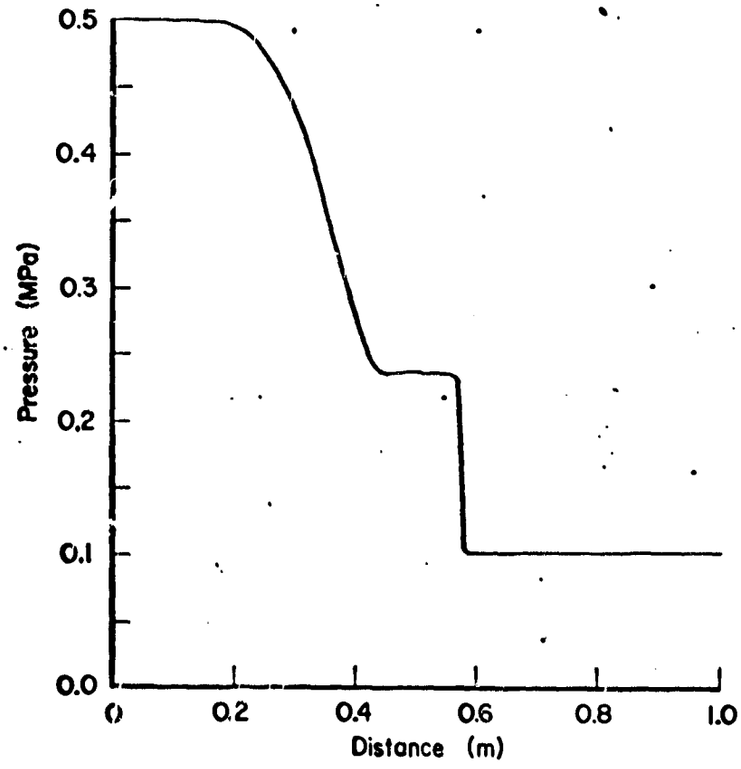

Fig. 3.6a. Pressure at t = 2 ms with condensation only.

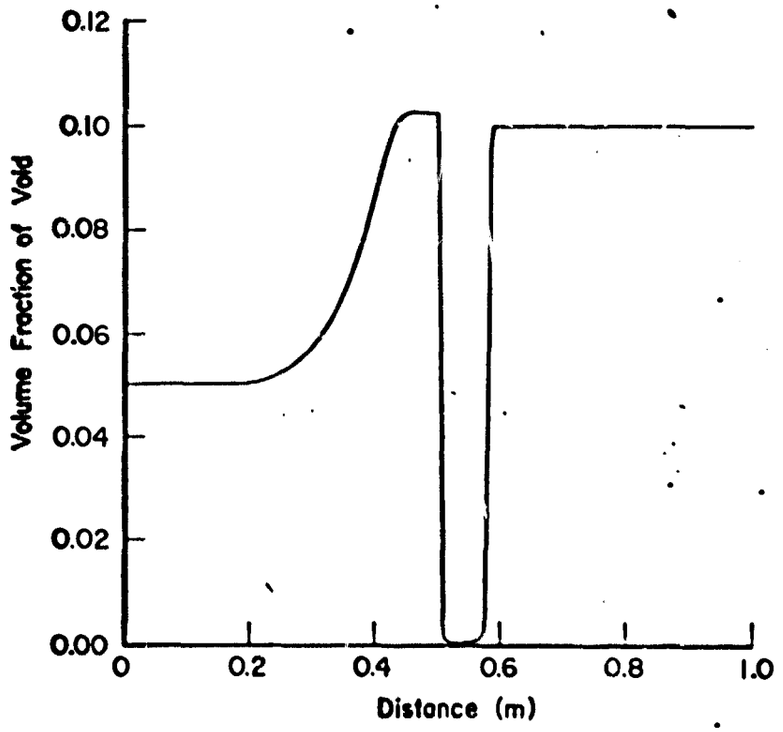

Fig. 3.6b. Volume fraction of void at t = 2 ms with condensation only.

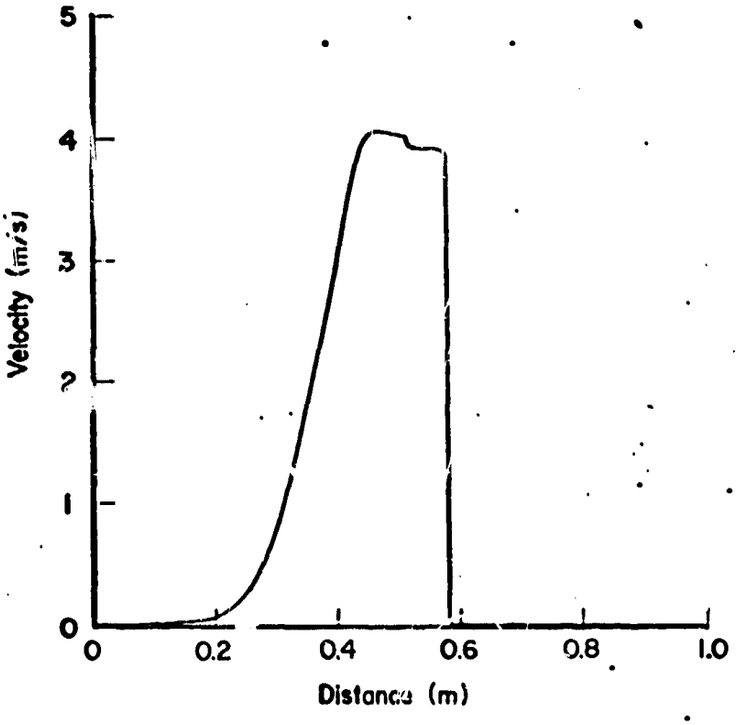

Fig. 3.6c. Velocity of liquid and gas at t = 2 ms with condensation only.

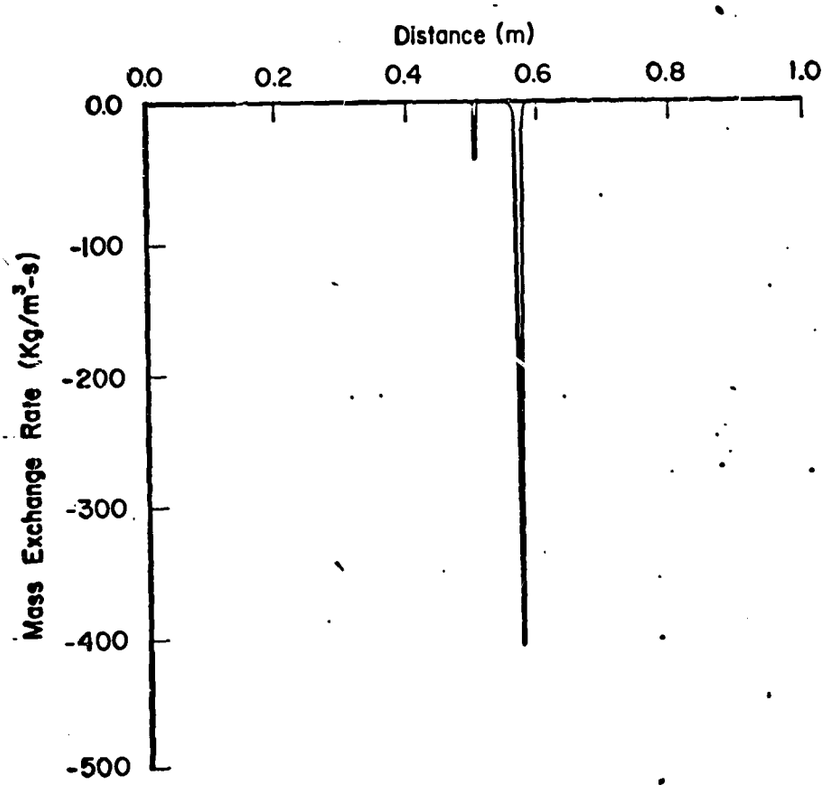

Fig. 3.6d. Mass exchange rate at t = 2 ms with condensation only.

3.7a

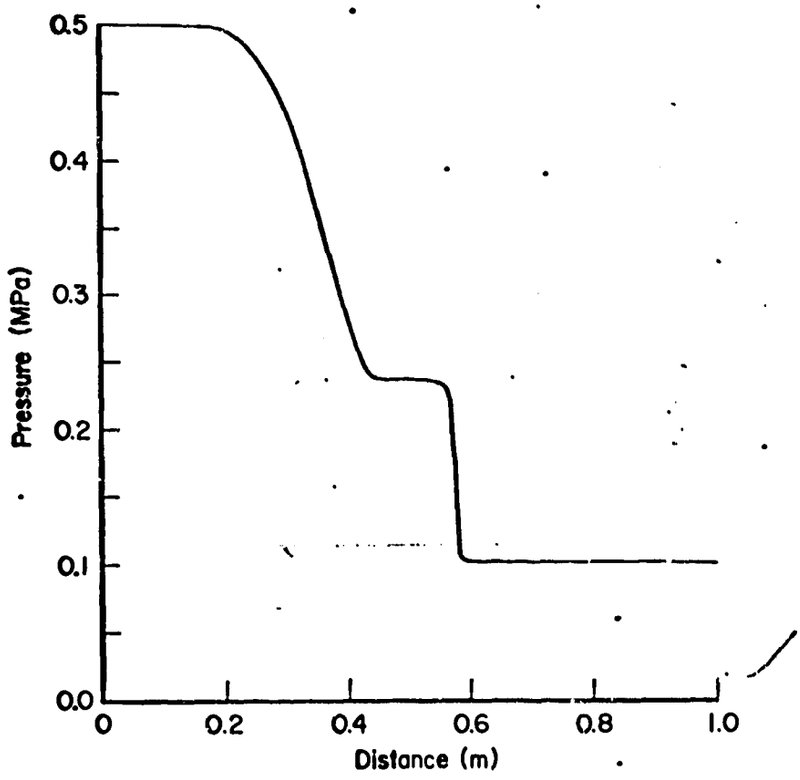

Fig. 3.7a. Pressure at t = 2 ms for $\lambda_c = 10$ with condensation only.

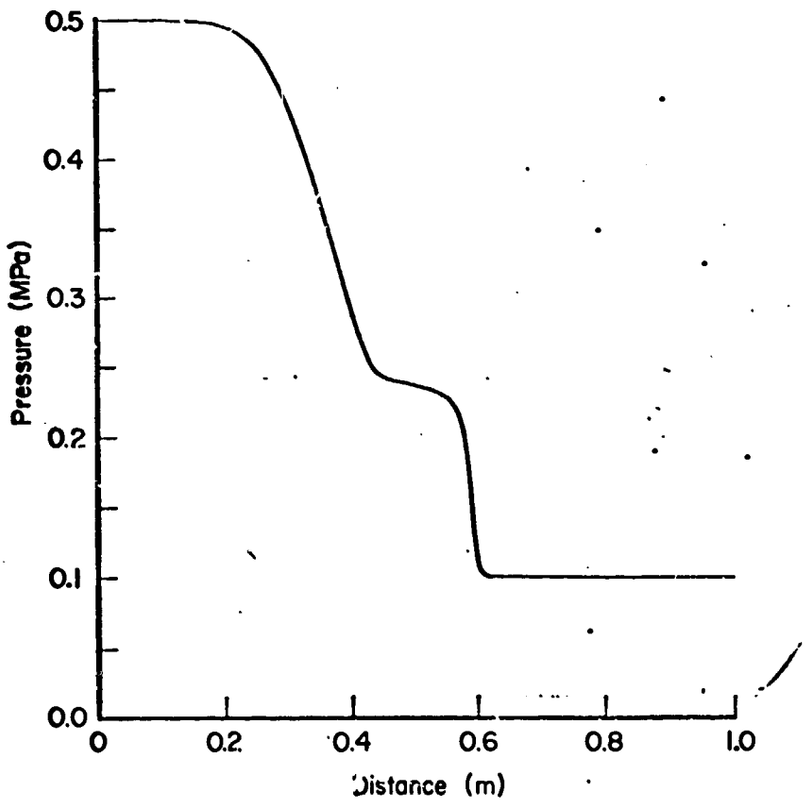

Fig. 3.7b. Pressure at t = 2 ms for $\lambda_c = 1$ with condensation only.

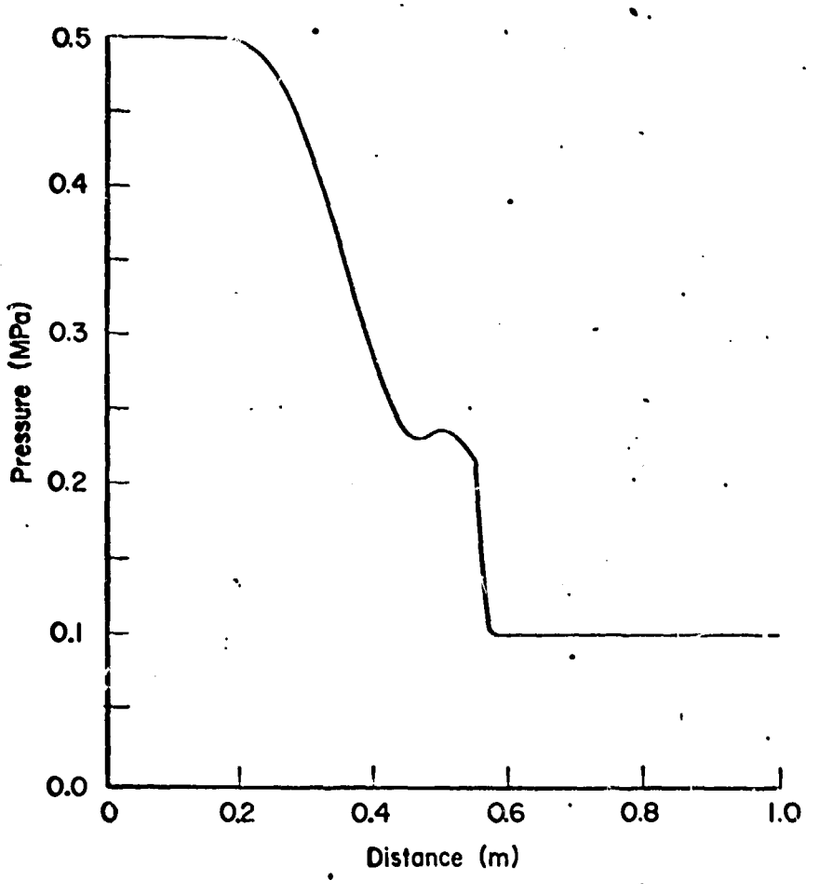

Fig. 3.8a. Pressure at $t = 2$ ms for $\delta t = 100\mu s$, $\delta z = 10$ mm with condensation only.

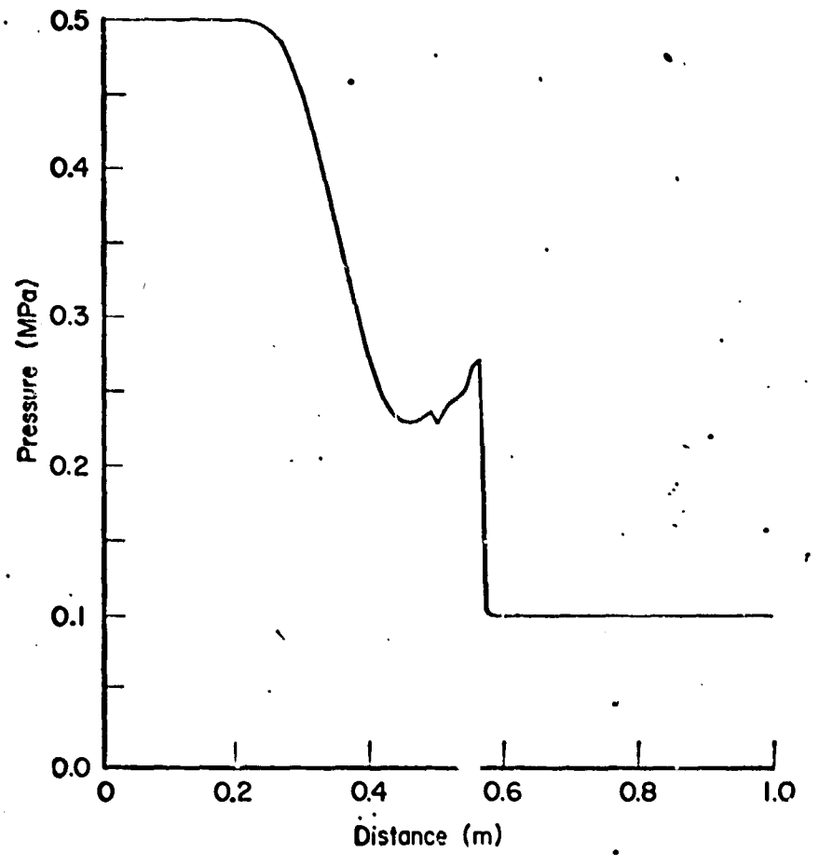

Fig. 3.8b. Pressure at $t = 2$ ms for $\delta t = 10\mu s$, $\delta z = 10$ mm with condensation only.

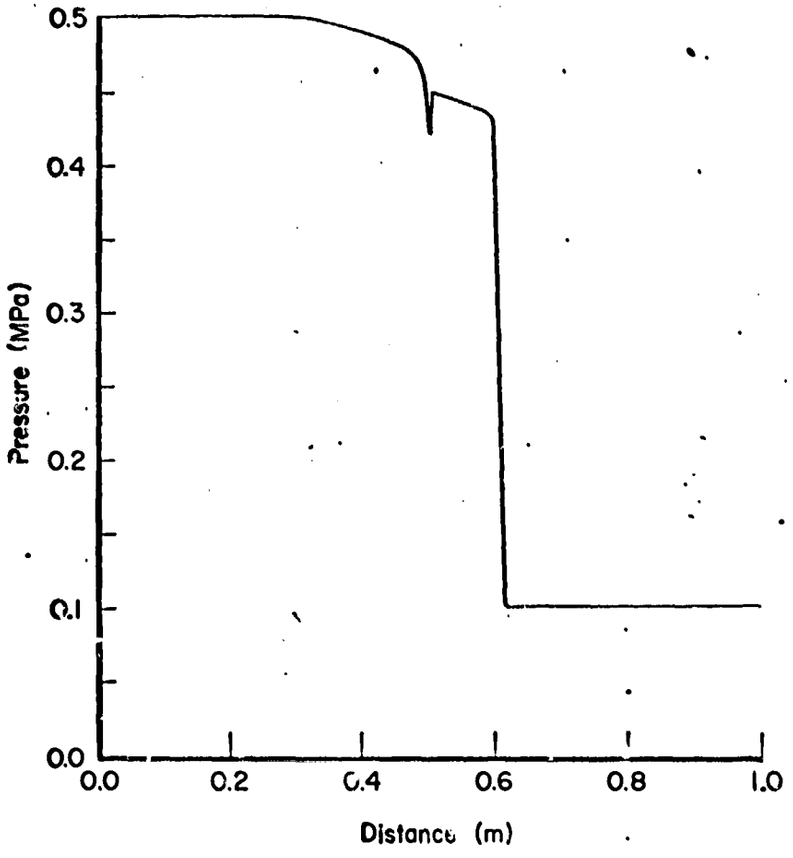

Fig. 3.9a. Pressure at t = 2 ms with boiling and condensation.

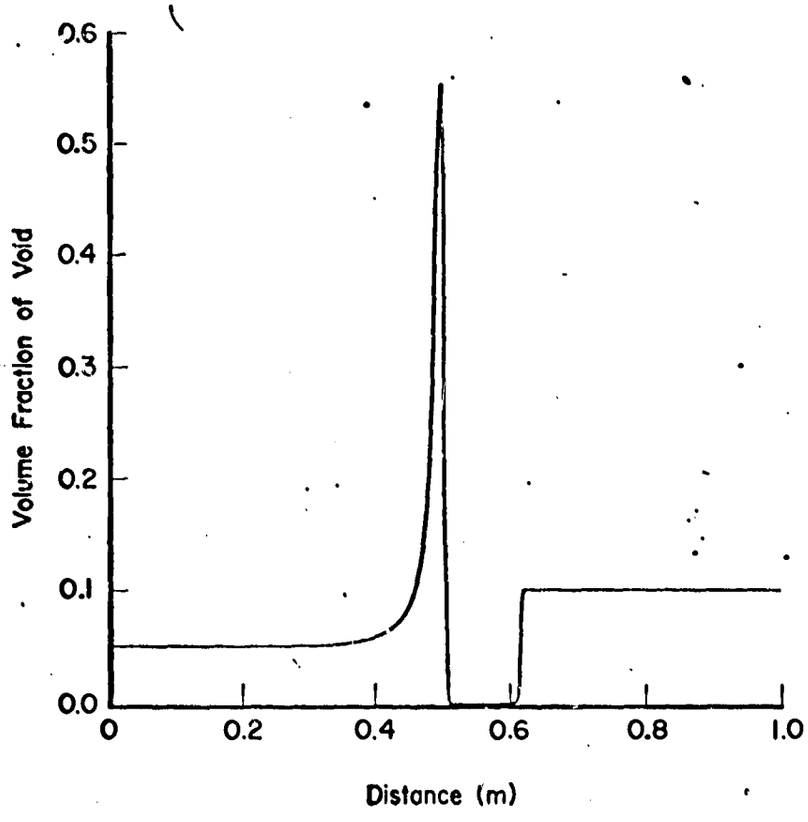

Fig. 3.9b. Volume fraction of void at t = 2 ms with boiling and condensation.

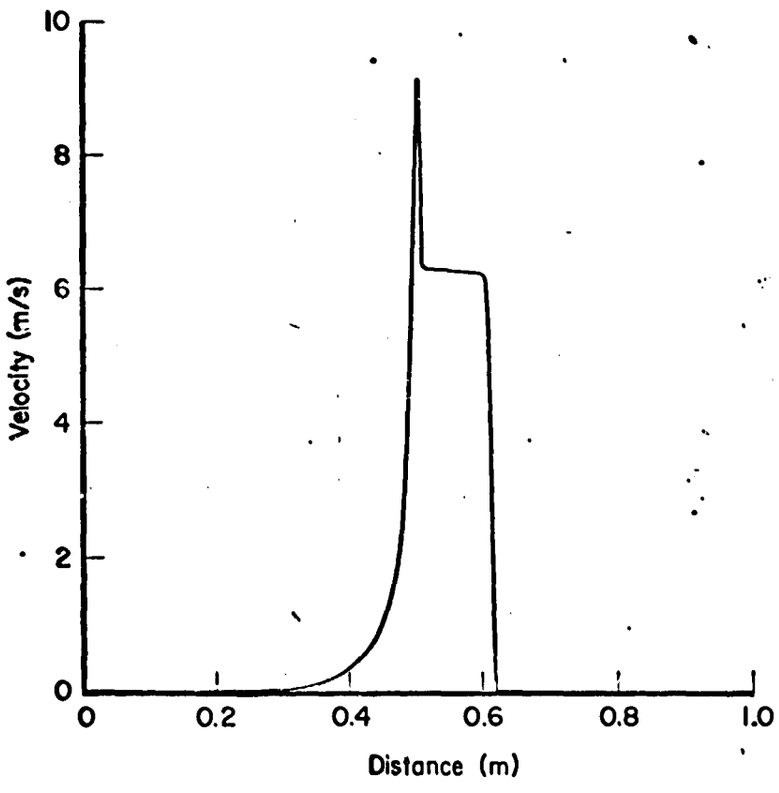

Fig. 3.9c. Velocity of liquid and gas at t = 2 ms with boiling and condensation.